

Easy, Scalable, Robust, Micropatterned Silk Fibroin Cell Substrates

Meng Xu, Sayantan Pradhan, Francesca Agostinacchio, Ramendra K. Pal, Gabriele Greco, Barbara Mazzolai, Nicola M. Pugno, Antonella Motta, and Vamsi K. Yadavalli*

Thin polymeric films are being explored for biomedical uses such as drug delivery, biofiltration, biosensors, and tissue regeneration. Of specific interest is the formation of mechanically flexible sheets, which can be formed with controllable thickness for sealing wounds, or as biomimetic cellular constructs. Flexible substrates with precise micro- and nanopatterns can function as supports for cell growth with conformal contact at the biointerface. To date, approaches to form free-standing, thin sheets are limited in the ability to present patterned architectures and micro/nanotextured surfaces. Other materials have a lack of degradability, precluding their application as cellular scaffolds. An approach is suggested using biocompatible and biodegradable films fabricated from silk fibroin. This work presents the fabrication and characterization of flexible, micropatterned, and biodegradable 2D fibroin sheets for cell adhesion and proliferation. A facile and scalable technique using photolithography is shown to fabricate optically transparent, strong, and flexible fibroin substrates with tunable and precise micropatterns over large areas. By controlling the surface architectures, the control of cell adhesion and spreading can be observed. Additionally, the base material is fully degradable via proteolysis. Through mechanical control and directing the adherent cells, it is possible to explore interactions of cells and the microscale geometric topography.

diffusion barriers, friction reduction, etc.^[1] Recently, such films and sheets have been explored for biomedical uses such as drug delivery, biofiltration, biosensors, wound healing, and tissue regeneration.^[2] Of specific interest are flexible, free-standing sheets, which can be formed with controllable thickness (ultrathin (tens of nanometers) to thin (few to tens of micrometers)). Sheets with mechanical flexibility and adhesiveness may be suitable for sealing wounds, or for the development of biomimetic cellular constructs. They can be stacked to form functional 3D tissues to form cell sheets as biomembranes or tissue/organ models.^[3] They can also be used as substrates for wearable devices, soft robotics, and smart skins.^[4] At the nanoscale thickness, such films can directly conform to the underlying surface, whereas at the microscale, adhesive layers may be needed for attachment to tissue.^[5]

Integrating thin films as dynamic cell culture platforms is of great interest because of applications in biosensing, regenerative medicine, and soft robotics.^[6]

Cell culture substrates capable of physically supporting cell growth with topographical and spatial cellular control can provide insight into the dynamics of cell interactions, while forming scaffolds and cell-based biosensors.^[6] A significant

1. Introduction

Thin polymeric films have long been used in industry for semiconductor applications, electronics packaging, as optical coatings,

Dr. M. Xu, S. Pradhan, Dr. R. K. Pal, Dr. V. K. Yadavalli
Department of Chemical and Life Science Engineering
Virginia Commonwealth University
601 W Main Street, Richmond, VA 23284, USA
E-mail: vyadavalli@vcu.edu


F. Agostinacchio, Dr. A. Motta
BIOTech Research Center
Department of Industrial Engineering
University of Trento
38123 Trento, Italy

G. Greco, Prof. N. M. Pugno
Laboratory of Bio-Inspired & Graphene Nanomechanics
Department of Civil
Environmental and Mechanical Engineering
University of Trento
38123 Trento, Italy

Dr. B. Mazzolai, G. Greco
Center for Micro-BioRobotics@SSSA
Istituto Italiano di Tecnologia
56025 Pontedera, Italy

Prof. N. M. Pugno
School of Engineering and Materials Science
Queen Mary University of London
London, E1 4NS, United Kingdom

Prof. N. M. Pugno
Ket-Lab
Eduardo Amaldi Foundation
00133 Rome, Italy

 The ORCID identification number(s) for the author(s) of this article can be found under <https://doi.org/10.1002/admi.201801822>.

DOI: 10.1002/admi.201801822

effort has been directed toward cellular micropatterning and organization.^[7] Spatial positioning of cells has been achieved using different techniques including patterning nonfouling chemistries (or complementarily, patterning of cell-attachment chemistries^[8]), plasma etching,^[9] microfluidic patterning,^[10] photolithography,^[11] soft lithography,^[12] inkjet printing,^[13] and microcontact printing.^[14] In addition, functionalization of the surface of substrates with proteins and enzymes has also been used to promote cell adhesion for orthopedic applications.^[15] However, it is often challenging to adapt these approaches beyond rigid or stiff substrates to flexible, mechanically robust sheets. Flexible substrates with precise micro- and nanopatterns can function as supports for cell growth, resulting in ordered and functional cell sheets that may be implanted, with conformal contact at the biointerface.^[16]

Flexible sheets may be formed using various techniques including casting elastomeric or intrinsically flexible materials, electrospinning, or by using spin coating or layer-by-layer assembly.^[2c] Paper has also recently attracted attention due to its porosity and flexibility, while permitting modifications of physical and chemical properties.^[17] Electrospinning to form micro- and nanofibrous architectures can form sheets (e.g., fiber mats) from a variety of synthetic and natural materials.^[18] However, imparting the additional property of patterned architectures (micro/nanotextured surface) has been limited, particularly over large areas (e.g., centimeter).^[19] Elastomers such as polydimethylsiloxane (PDMS) and polyurethanes have been used with favorable properties including high optical transparency, ability to form micropatterns, and control of stiffness.^[20] Despite good biomimetic characteristics and tunable mechanical properties, these materials have high surface hydrophobicity, limited aqueous processing, and, importantly, a lack of degradability, which precludes their application as cellular scaffolds.

Recently, approaches toward forming flexible, micro- and nanopatterned substrates have been reported. Using pNIPAM as a sacrificial layer, thin polystyrene (PS) films were spin-coated and stamped with cell adhesive carbon nanotube–fibronectin composites using microcontact printing (μ CP) to guide C2C12 skeletal myoblasts.^[21] Ultrathin poly(methyl methacrylate) (PMMA) films were formed using a similar spin-coating procedure and micropatterned with cell-adhesive poly(L-lysine) using inkjet printing.^[22] However, both PS and PMMA are nonbiodegradable polymeric materials, limiting their applications. Using degradable polymers such as poly(lactic acid) (PLA),^[23] chitosan, and alginate,^[24] free-standing films have been reported. An important report using self-assembled chitin nanofiber substrates micropatterned using replica molding for engineered cell sheets was shown.^[25] These flexible substrates are biodegradable, mechanically strong, and can be manipulated into desired shapes. However, stamping procedures have limitations that can affect pattern resolution and reproducibility including deformation scalability over large areas, and ink mobility to unwanted regions.^[26] Nonetheless, these interesting studies have shown the way for forming flexible, micropatterned sheets for various applications.

Herein, an approach is suggested using silk protein films. Silk as a natural biopolymer to fabricate various geometries to support the cell regeneration and tissue repair has been widely

examined for the past few decades.^[27] The silk protein fibroin possesses high mechanical strength and flexibility, optical transparency, biocompatibility, low immunogenicity, permeability to water and oxygen, and, importantly, biodegradability.^[28] Fibroin, either by itself, or in conjunction with other materials, has been electrospun into films and mats for cell culture.^[29] Micropatterned silk films prepared by molding were earlier reported.^[30] In these experiments, different surface groove patterns were prepared from optically graded glass substrates followed by casting poly(dimethylsiloxane) replica molds. However, patterns that can be formed are not easily scalable and cannot recapitulate complex designs owing to the need to form transfer molds. In earlier work, our group reported the use of biochemically modified silk proteins (fibroin and sericin) that behave as negative tone photoresists for optical, electrochemical, and biomedical applications.^[31] In these forms, silk proteins can be micropatterned using a facile, benchtop photolithographic technique, allowing the formation of microarchitectures on rigid or flexible substrates. High resolution at micro- and nanoscales, high throughput, and excellent reproducibility are achievable.

In this study, we demonstrate flexible, strong, micropatterned, and biodegradable 2D silk fibroin sheets for the adhesion and proliferation of cells. We show a rapid and scalable technique using photolithography to fabricate optically transparent, flexible fibroin substrates with tunable and precise micropatterns over large areas. To the best of our knowledge, this is the first report of a flexible, micropatterned cell culture substrate using photolithography combined with degradable natural or synthetic biopolymers. By controlling the surface architectures of these flexible sheets, the control of cell adhesion and spreading can be observed. The technique presented in this study is simple, requiring no clean room or strong reagents, and permits rapid engineering of mechanically robust sheets with a variety of topographic features and length scales. Since the structures are formed independently of the substrates, it is possible to form surface patterns of different mechanical properties from the underlying support. Additionally, since the base material is fully degradable via proteolysis, it provides a promising platform for the formation of cell sheets. Through mechanical control and directing the adherent cells, we can further explore the interactions of the cells and the microscale geometric topography.

2. Results and Discussion

2.1. Fabrication of Flexible, Micropatterned Fibroin Films

Mechanically flexible, biocompatible sheets present platforms for applications as surface biosensors, soft robotics, drug delivery vehicles, sealing of wounds, and tissue scaffolds.^[2c] The presence of micropatterns can further provide opportunities to direct the behavior of cells or control cell morphology in situ.^[32] To date, micropatterned films have been shown on rigid or supported formats (for instance, with an underlying glass or polystyrene substrate) or using flexible materials that are not degradable (e.g., PDMS). The development of flexible, and micropatterned films and membranes using degradable biopolymers has been limited.^[24] In this work, microfabrication

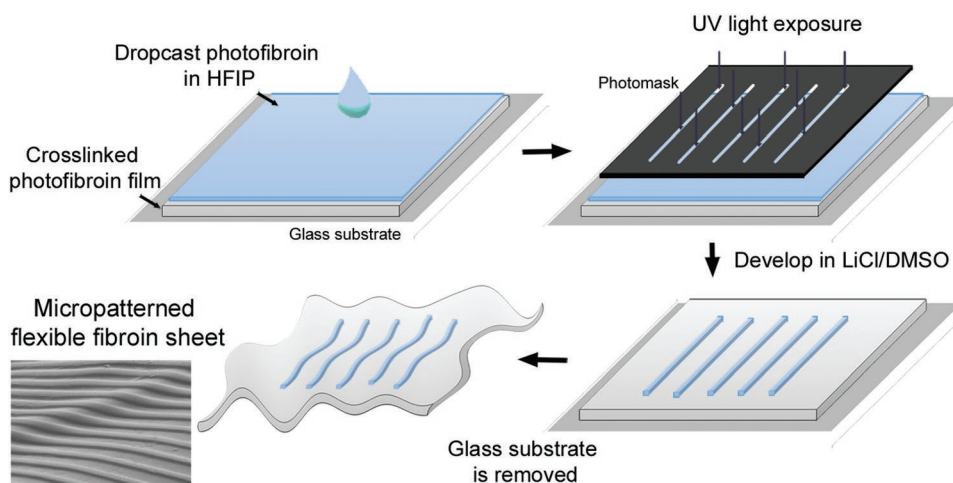


Figure 1. Fabrication of micropatterned flexible fibroin films via photolithography.

of flexible, silk fibroin films is realized using light-reactive conjugates and facile photolithographic techniques.^[31] These conjugates can be used as stable, biodegradable, and biocompatible substrates on which patterns are formed. Previously, patterns of sericin were shown on flexible fibroin substrates, which could be accomplished since the two are soluble in different solvents (viz. sericin in water, fibroin in formic acid or HFIP). Here, we utilize fibroin as the material comprising both the substrate and the pattern. The use of photolithography provides a rapid route to form complex patterns that are not easily prepared using microcontact printing or molding.^[30]

Initially, a solution of photo-crosslinkable silk fibroin in formic acid with a suitable photoinitiator was cast on a plain glass slide (1 cm² area) and crosslinked by exposure under 365 nm UV light (**Figure 1**). The use of formic acid as a solvent allows us to form large scale, thin, flat, and stable fibroin films in an environmentally friendly process.^[31b] These films are formed by crosslinking of the protein and not by a change in β -sheet conformation as shown in other works.^[32,33] The UV crosslinked fibroin sheets formed are water insoluble and are stable in a wide range of solvents. Due to the absence of chemical linkage between the film and the glass support, the crosslinked fibroin sheet can be easily peeled off when immersed in water. The thickness of the film plays a defining role in its flexibility, and films ranging from hundreds of nanometers to tens of micrometers are easily formed by controlling the amount of fibroin/formic acid solution cast and the spin-coating speed. For example, 60 μ L of fibroin solution cast on a plain glass slide of area 1 cm² produces films with a thickness \approx 10 μ m at a spin speed of 800 rpm.

To fabricate microarchitectures of silk fibroin photoresist on fibroin films, a 5% w/v solution in HFIP was cast on silk fibroin sheets prepared as described above. The presence of residual acrylate functional groups on the surface of the films enables the covalent attachment of patterns on them. This implies that the patterns do not delaminate when the film is subjected to mechanical deformation. Patterns are formed by exposure to 365 nm UV through a photomask (**Figure 1**). The area exposed by the UV light is crosslinked while, the unexposed areas

dissolve when immersed in 1 M of LiCl in DMSO. A wide range of patterns with different shape, size, and complexity can be obtained depending on the nature of the photolithographic mask used. The use of a single material for the fabrication of the substrate and the patterns allows us to form microarchitectures of high stability due to the presence of the same chemistry. Due to the volatility of HFIP, a solution of photofibroin in HFIP can be cast on the fibroin films without disrupting the underlying film. This demands precise control over the amount of solution drop cast on the fibroin films and drying time prior to UV exposure for patterning. 30 μ L of FPP/HFIP solution for a fibroin film of area 1 cm² and a drying time of \approx 5 min was found to be optimum for the results shown here. Once they are immersed for development, the entire structure can be delaminated from the glass support to form mechanically flexible films (**Figure 2a**). The images obtained from an optical microscope show the ability to form ordered patterns of various complexities over a large area (centimeter scale) of flexible fibroin sheet (**Figure 2b,c**). Thin, moist films can be applied to and readily conform to irregular surfaces (e.g., skin) without the need for any adhesive (**Figure 2d**). The films can also be attached in a dry condition to a curved surface (**Figure S1**, Supporting Information).

The micropatterned films are mechanically robust (strength > 100 MPa, **Figure 2e**) and can be held, rolled, or bent into various conformations numerous times without any loss in their chemical and physical properties. A video showing the tensile behavior of the films is provided in the Supporting Information. The films are stronger than the earlier reported micropatterned chitosan films.^[25] To demonstrate the structural integrity and scalability at the microscale, optical and scanning electron microscopy (SEM) images were taken. The SEM images (**Figure 3**) depict the high fidelity and spatial and structural resolution of the micropatterns as lines or dots. Due to the vinyl linkage between the patterns and the substrate, a strong adhesion is observed at the interface and the structures are intact even in bent conditions. In **Figure 3c,d**, the film was examined before and after conducting several (\approx 10 times) extreme 180° bends. While some minor cracks may be seen

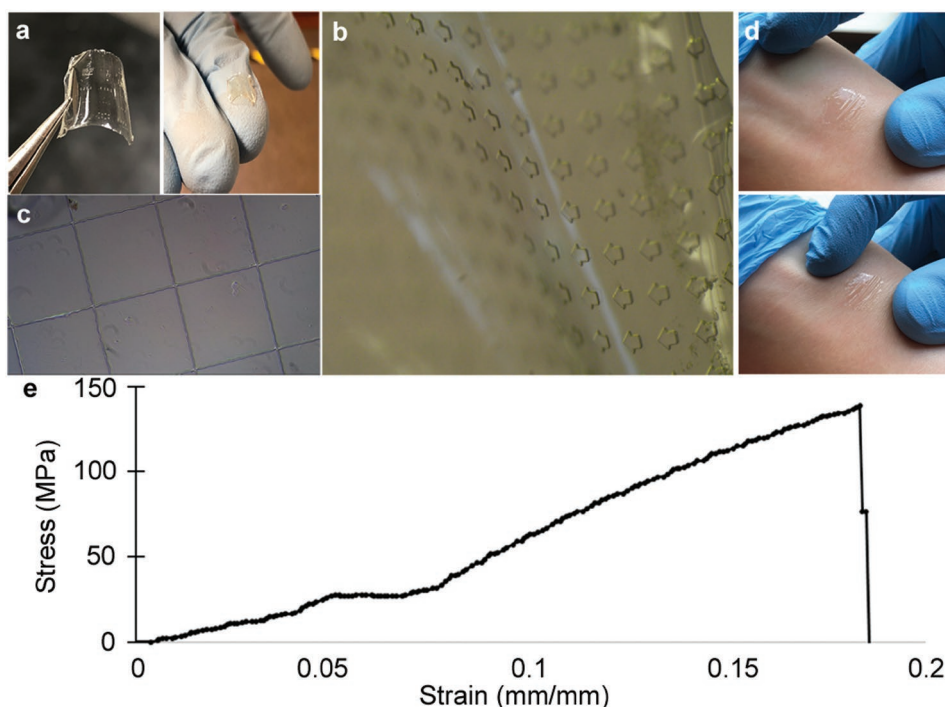


Figure 2. a) Mechanically stable micropatterned films formed by photolithography. Large area films can be patterned with microscale architectures b). c) Optical image of the films shown after sterilization with 70% ethanol. d) Ultrathin micropatterned films (<math><1\ \mu\text{m}</math>) can be easily applied to soft surfaces (e.g., skin) without any adhesive—shown in stretched and squeezed forms. e) Stress–strain curve of the substrate (dry condition), showing a strength >100 MPa.

on the film at the bend junction, the patterns themselves do not delaminate, demonstrating the high robustness of this system. This can be correlated to the differences in terms of

Young modulus between the softer pattern and the stiffer substrate (Figure 4a–c) which are observed under nanoindentation. Under mechanical deformation, the former is thus more

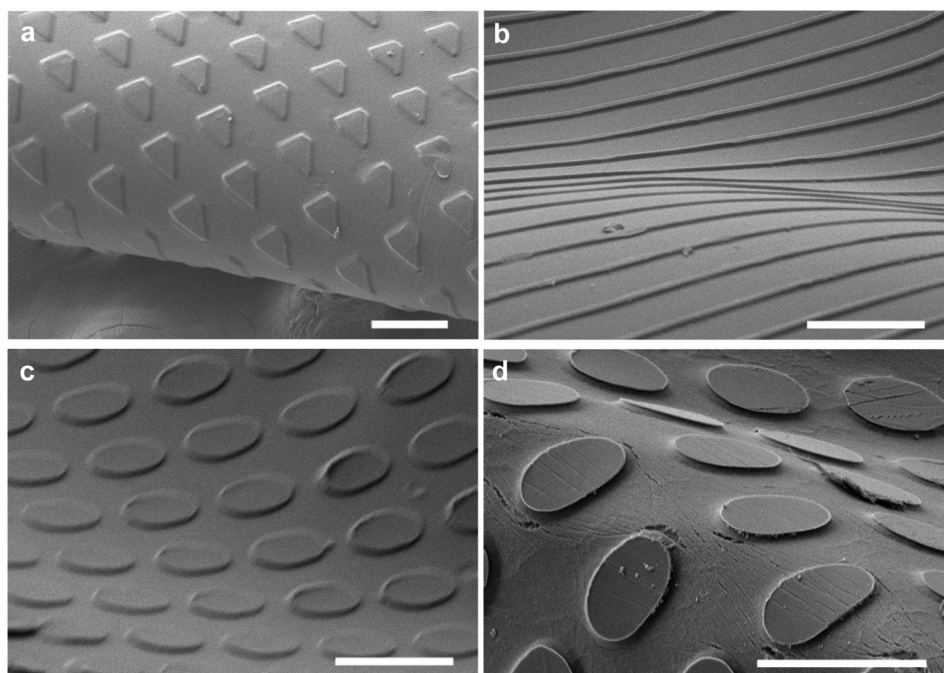


Figure 3. SEM images of the different forms of flexible microstructured films of silk fibroin fabricated by photolithography a) films can be fully rolled, b) different kinds of surface architectures are easily patterned using different photomasks. Image taken before c) and after d) repeated 180° bends shows nanoscale cracks but the film integrity is preserved and no delamination of features observed. Scale bar on all images = 100 μm .

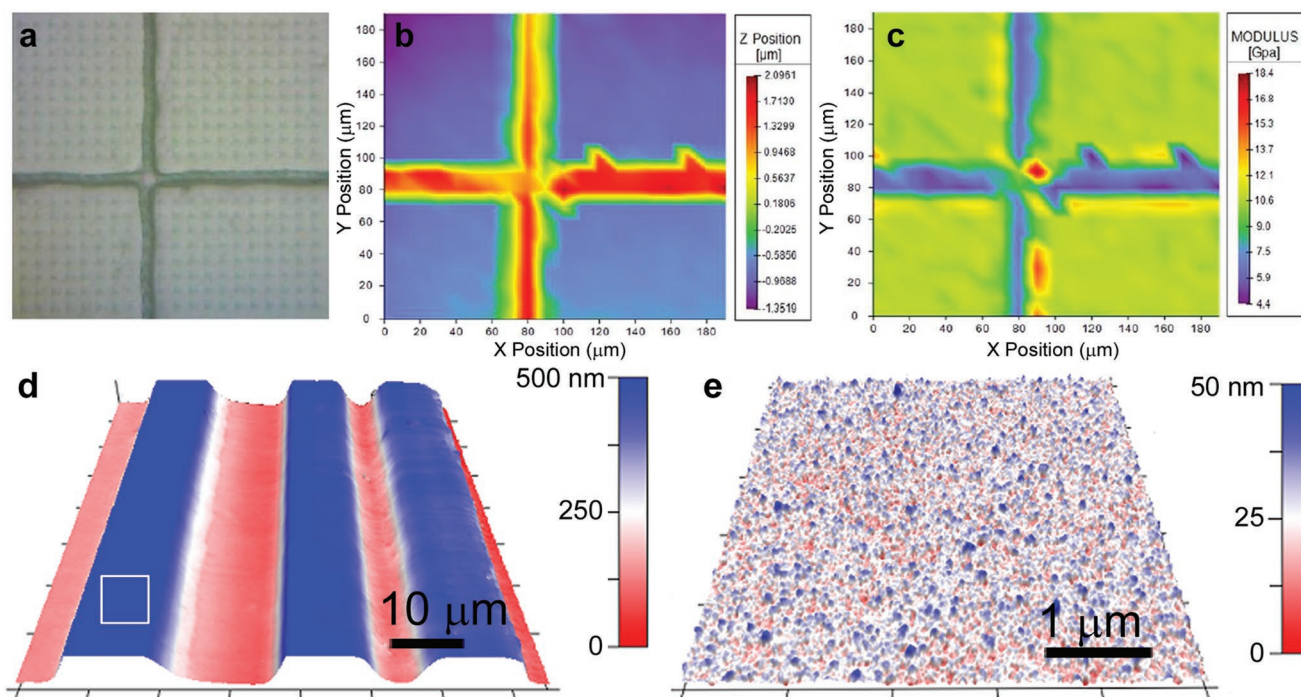


Figure 4. Spatial distribution of the localized mechanical property and imaging of the patterned surface. a) The optical microscope image of the surface following nanoindentation. b) Z-position of the indenter indicating the pattern height, and c) Young's modulus spatial distribution, showing the softer pattern on the stiffer underlying substrate (scales on all panels are same). d) AFM imaging of the fibroin micropatterns on fibroin films: 75 μm scan of 10 μm lines separated by 25 and 5 μm gaps. The patterns are 500 nm in height. e) Scan of a 5 \times 5 μm area from the flat region of the line shows the flat nanosurface of the films (RMS roughness \approx 5 nm over this area).

flexible with respect to the latter, adapting itself to the deformation of the substrate. The load–displacement curves obtained by nanoindentation of the patterned films and spatial distribution of the surface mechanical properties are presented in Table S1 and Figures S2 and S3 in the Supporting Information.

AFM imaging of the films (Figure 4d,e) show that they are smooth at the nanoscale (both on the film and on the surface of the patterns) with a root mean square (RMS) roughness \approx 5 nm over a 5 μm area. In this case, the films used for cell culture with patterns of 10–25 μm were imaged. In these films, the patterns were around 500 nm in height, fabricated via spin coating. Similar patterned films were used for cell culture as discussed below. The lines have a high structural fidelity and resolution demonstrating the accuracy of this photolithographic process to form micropatterns over large areas. Patterns down to \approx 3 μm using benchtop lithography are easily formed (Figure S4, Supporting Information). Nanoscale patterning using electron beam lithography was previously demonstrated by our group and could potentially be extended to this system. Due to the optical transparency of the entire structure, they can also find their application in optics for the fabrication of soft and flexible optical systems.

2.2. Proteolytic Degradation of Fibroin Substrates In Vitro

An advantage in using natural biopolymers is that devices fabricated based entirely on these materials can be degraded in physiological environments. The silk fibroin biomaterial used

in this study enables controllable biodegradability of the flexible devices. Under the reaction of protease, the micropatterned sheets are degraded, ultimately leading to the loss of mass and structural integrity. An enzymatic biodegradation experiment was conducted on micropatterned films incubated in phosphate buffer saline (PBS) solution with or without protease (control) at 37 $^{\circ}\text{C}$. The percentage of mass weight remaining (obtained as W_t/W_0) was recorded to observe the overall decomposition of the films ($n = 3$) over time (Figure 5). No significant mass loss was observed when incubated in PBS over the 2 week period. Due to proteolytic biodegradation, a gradual loss of weight was

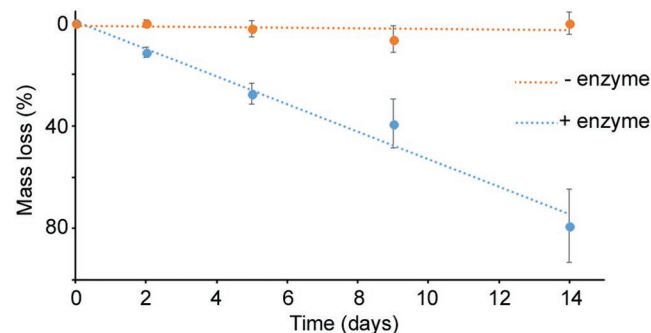


Figure 5. Proteolytic degradation of micropatterned fibroin films. The films are stable in buffers (solution containing no enzyme was used as the control denoted as –enzyme), but show significant mass loss in the presence of protease (+enzyme), ultimately breaking down completely within 3 weeks. (Sample size $n = 3$ films for each experiment)

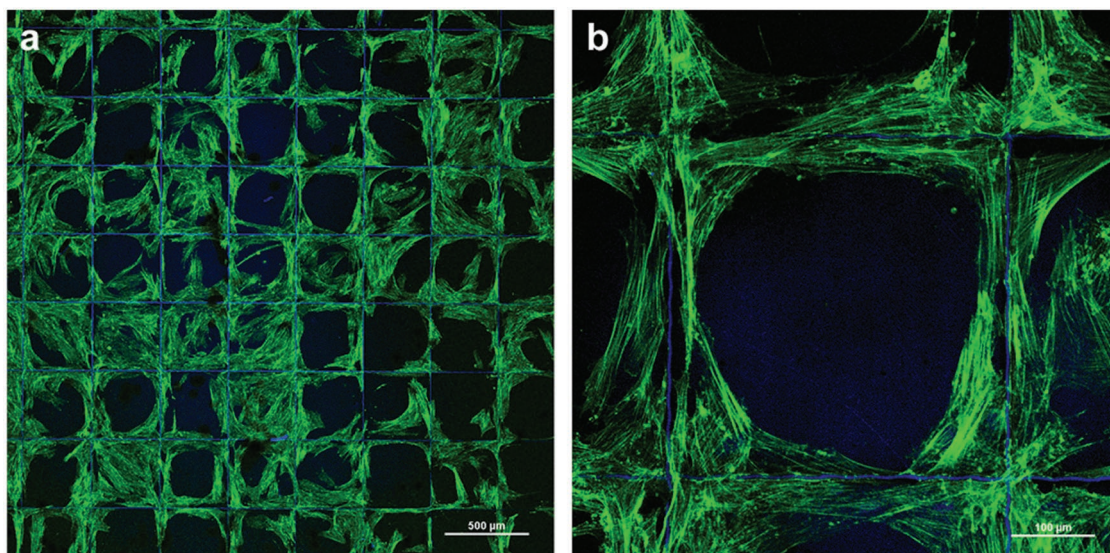


Figure 6. a) Contact guidance of fibroblasts on flexible fibroin films patterned with square grids (10 μm thick lines) as observed by confocal microscopy. The dark regions represent the film without any pattern. Images of hBM-MSCs cytoskeleton organization stained with Oregon Green 488 at day 8. Blue (DAPI) was completely absorbed by the films and used to show the grid-like shape pattern. Scale bar = 500 μm . b) Close-up showing the actin filaments attached to the underlying substrates. Scale bar = 100 μm .

observed and <40% of the weight remained after 14 days of incubation. After 14 days, the films incubated in the enzyme broke down, whereas the control samples maintained their integrity and flexibility. This was consistent with previously reported observations in which the biodegradability of fibroin based flexible devices can be tuned by controlling the degree of crosslinking and film thickness.^[31,34] Therefore, devices with precisely engineered lifetimes can be fabricated using these micropatterned films, which can be useful as implantable bioelectronics and tissue scaffolds.

2.3. Evaluation of Cell Adhesion

Unlike earlier reported cell patterning approaches, wherein cell adhesive regions are obtained by stamping, inkjet printing, proteins etc.,^[8e,15,22] here spatial position is controlled through the use of surface micro/nanoarchitectures. To verify the impact of fibroin patterning on cell adhesion, human bone marrow-multipotent stromal cells (hBM-MSCs) were studied on the flexible fibroin sheets. The micropatterns and films are robust enough to withstand the sterilization procedure (Figure 2c). Three different conditions were explored on sheets micropatterned with square grids—unmodified sheets, preconditioning with expansion media, and coating with fibronectin. After 8 days of culture, the cytoskeleton was stained with Oregon Green and observed by confocal microscopy imaging. However, cells exhibited a low proliferation and nonspecific adhesion to unmodified sheets. In the case of pretreatment in expansion medium, films showed higher cell adhesion when compared with untreated sample, with preferential attachment to the fibroin patterns (Figure S5, Supporting Information) even if all sample surfaces were incubated in culture medium or fibronectin. At higher

magnification, the alignment of the cytoskeleton on fibroin pattern coated with human fibronectin can be clearly seen. Note that multiple replicates (3–5 films for each condition) were performed. The results obtained on preconditioned with complete expansion medium and unmodified films were also useful, showing that despite the low adhesion, the films themselves are not cytotoxic.

Figure 6 shows cells on films coated with human fibronectin. DAPI was completely absorbed by the films and used only to show the underlying organization of the grid patterns. This condition had the highest proliferation rate and organization of the cells. The cells clearly align according to the design of the grid patterns. Most interestingly, in addition to the adhesion of the cells to the grid organization (Figure 6a), the cells were able to migrate from grid to grid eventually filling up the sheet (Figure S6, Supporting Information). Note that the height of the grids is ≈ 500 nm in these sheets. This data suggests a significant role of the fibronectin coating, that together with pattern organization is able to guide and enhance cellular growth and proliferation according to a specific designed order. It is clear that the topographical features of the fibroin pattern produced on a fibroin film still allow cell adhesion primarily along the patterns. The cells are therefore guided almost exclusively by the surface morphology, and to some extent, the stiffness differences between the pattern and the substrate. In these films, the patterns are less stiff in comparison to the substrate (Figure 2e). The ability to modulate the stiffness of the patterns is another advantage of this technique in comparison to molding techniques which form mechanically homogeneous films. Such flexible, cell culture sheets can therefore be used for fundamental studies of 3D tissue models and scaffolds, where the micropatterns can be used to guide cells initially, and the underlying sheets eventually degrade over time.

3. Conclusions

In summary, here we demonstrate the facile fabrication of micropatterned, free-standing films of the silk protein fibroin that are flexible and can be used for controlling cellular organization. The films themselves are mechanically robust, can be formed at various thicknesses ranging from ultrathin (<1 μm) to thick (tens of micrometers), and can be controllably degradable. The surface of these films can be tailored by decorating with patterns of silk fibroin using a photolithographic technique, which permits the formation of complex, high resolution architectures at high throughput and scale (over several centimeters). Virtually any structural pattern can be easily and rapidly formed using light-assisted microfabrication. The cell-adhesive micropatterns were shown to spatially direct cells. In addition to the patterns, it is also possible to modulate the mechanical characteristics of the patterns. These results suggest that micropatterned silk sheets can provide a bioinspired and biodegradable structure toward the flexible cell culture platforms and devices.

4. Experimental Section

Synthesis of Photo-Crosslinkable Fibroin: Silk fibroin was extracted from silk cocoons using a standard protocol.^[35] Fibroin protein photoresist (FPP) was prepared by the incorporation of photoreactive moieties to the fibroin structure as reported earlier.^[30a] Briefly, pure fibroin was dissolved in 1 M LiCl/DMSO and reacted with 2-isocyanatoethyl methacrylate (IEM) in stoichiometric amounts for 5 h at 60 °C, while maintaining inert conditions using a constant flow of nitrogen. After the completion of the reaction, the product mixture was added to cold ethanol, and the methacrylated protein was obtained as the precipitate. The product was washed with a 1:1 ratio of cold ethanol and acetone followed by centrifugation and lyophilization for 24 h to obtain the fibroin protein photoresist (photofibroin) powder.

Fabrication of Flexible Micropatterned Fibroin Films: The flexible micropatterned substrate was fabricated by dissolving 7.5% w/v of photofibroin in formic acid (Acros Organics 98%). 2.5% w/v photoinitiator (Irgacure 2959, BASF) was added. The solution was drop cast on plain glass slides and air dried for 15–20 min in order to evaporate the excess solvent. The samples were exposed under a 365 nm UV lamp (Lumen Dynamics OmniCure 1000 system) for 3 s at 20 mW cm^{-2} for crosslinking. To create fibroin films, the samples were dipped in deionized (DI) water which facilitated the delamination from the glass. Micropatterns of silk fibroin were fabricated on these films using contact photolithography. Films prepared as discussed above were used as the substrates. A 5% w/v solution of FPP in 1,1,1,3,3,3-hexafluoro-2-propanol (HFIP, Sigma-Aldrich, St. Louis, MO) was drop casted on fibroin films. The samples were air dried for 5 min, allowing the HFIP to evaporate. Micropatterned structures were formed by placing a photolithographic mask with the desired array of patterns on the substrates and exposing it under UV irradiation for 1.6 s. Patterns were developed by immersing the samples in 1 M LiCl/DMSO solution for \approx 2 h. The patterns were then rigorously cleaned with DI water to wash off any un-crosslinked material and excess LiCl/DMSO solution.

Proteolytic Degradation In Vitro: Micropatterned fibroin films can be proteolytically degraded over time in the presence of enzymes. In the present work, the degradation of fibroin microstructures on films in the presence of protease (Protease XIV from *Streptomyces griseus*, ≥ 3.5 U mg^{-1} , Sigma Aldrich) was studied. Films (containing ≈ 2.5 mg fibroin) were incubated in 5 mL protease (1 U mg^{-1} of protein) at 37 °C and the degradation was studied over 2 weeks. Another set of samples were incubated in PBS buffer under the same environment, which served as the negative control (NC). The enzyme solution was replaced every 3 days to maintain the activity of protease. Samples from each set were

taken out on different days, rinsed with DI water, dried under N_2 , and weighed to record their degradation over time. Degradation over time was characterized as a function of mass loss of the films.

In Vitro Cell Culture: Human bone marrow-multipotent stromal cells were cultured in expansion medium consisting of DMEM:F12 (Euroclone), supplemented with 10% fetal bovine serum (Euroclone), 1% antibiotic antimycotic (Euroclone). Cells were cultured in 75 cm^2 flask at 37 °C and 5% CO_2 in humidified atmosphere. Medium was changed twice per week and when at 80% confluence, were detached with trypsin-EDTA (Euroclone). For this study cells were used at passage 3.

Fibroin films prepared as discussed above were sterilized with 70% ethanol for 45 min and then washed twice with sterile distilled water to completely remove ethanol. To improve cell adhesion, one set of samples was preconditioned in complete expansion medium for 20 min at 37 °C, and the second set incubated in human fibronectin (Sigma) 10 $\mu\text{g mL}^{-1}$ in PBS for 1 h at 37 °C. As a control, films without any treatment as well as cells seeded on tissue culture plate well (TCP) were used. Cells were seeded at 3×10^4 cells mL^{-1} on each sample. 1 mL of cell suspension was seeded. After seeding, cells were left to adhere for 1 h before adding fresh medium. Cells were then cultured up to 8 days.

Morphological Evaluation of Adhered Cells: Cell morphology and organization on patterned films were studied by imaging at day 8 after seeding using confocal microscopy. Prior to imaging, adhered cells were fixed with 4% PFA for 40 min, and then permeabilized with 0.2% Triton X-100 for 40 min. To investigate nuclear and cytoskeleton organization of cells on films, hBM-MSCs were stained with DAPI (Sigma-Aldrich) for nucleus and Oregon Green 488 (ThermoFisher) for actin filaments according to manufacturer's instructions for 15 min. Samples were examined using a Nikon A1 Confocal Laser Microscope.

Imaging and Nanoindentation: Imaging of the substrates was conducted using atomic force microscopy (AFM) via an MFP-3D AFM (Oxford Instruments, Santa Barbara, CA). Si_3N_4 cantilever (Olympus) with a nominal spring constant of $k = 2$ nN nm^{-1} was used for noncontact imaging in air. For mechanical characterization, nanoindentation was conducted using an iNano Nanoindenter (Nanomechanics Inc.) equipped with a Berkovich tip. The tested samples were prepared by affixing the film on a stub. The declared sensitivity of the machine was 3 nN for the load and 0.001 nm for the displacement. A mapping method (Nanoblitz 3d, Nanomechanics Inc.) was used, with a nanoindentation grid of 200 $\mu\text{m} \times 200 \mu\text{m}$ square with 400 indentation points inside and maximum load of 15 mN. The standard indentation method was used at 15, 30, and 45 mN maximum load to analyze the influence of the applied force. The standard indentation method with 45 mN maximum load was applied at different positions on the substrate to analyze the variation of the Young modulus on the film surface. The comparison of the data (Figure 3c) was performed by using T-statistics and the taken quantile was 2.021 by considering more than 40 degrees of freedom.

Tensile Tests: Samples were prepared by fixing on a paper frame provided with a square window of 0.5 cm side. The sample was fixed to the frame using double-sided tape and a high-strength glue. For fracture tests, a MIDI 10 machine with a load cell of 10 N and imposed velocity of 0.1 mm s^{-1} (strain rate of 0.02 s^{-1}) was used. The cyclic tests and the Young's modulus measurements were performed with the nanotensile machine Agilent UTM T150 (Keysight Technologies, CA), with a load cell of 500 mN and a displacement speed of 1 $\mu\text{m s}^{-1}$. The tests were recorded with a Sony Camera (video showing the tensile test is provided in the Supporting Information).

Additional images of the microstructures, cellular spreading, mechanical testing data (load–displacement curves for indentation, Young's modulus distribution) as well as tensile stretching of the samples are provided in the Supporting Information.

Supporting Information

Supporting Information is available from the Wiley Online Library or from the author.

Acknowledgements

This research was partly supported by funding from the National Science Foundation (CBET-1704435). V.K.Y. acknowledges support from the Core Fulbright Scholar program for 2017–18. SEM images were obtained at the VCU Nanomaterials Characterization Center. N.M.P. was supported by the European Commission under the Graphene Flagship Core 2 Grant No. 785219 (WP14 “Composites”) and FET Proactive “Neurofibres” Grant No. 732344 as well as by the Italian Ministry of Education, University and Research (MIUR), under the “Departments of Excellence” Grant L. 232/2016 and ARS01-01384-PROSCAN.

Conflict of Interest

The authors declare no conflict of interest.

Keywords

biodegradable, flexible cell sheets, micropatterning, protein photolithography, silk fibroin

Received: November 14, 2018

Revised: February 10, 2019

Published online:

- [1] a) J. A. Forrest, K. Dalnoki-Veress, *Adv. Colloid Interface Sci.* **2001**, 94, 167; b) C. M. Stafford, C. Harrison, K. L. Beers, A. Karim, E. J. Amis, M. R. VanLandingham, H.-C. Kim, W. Volksen, R. D. Miller, E. E. Simonyi, *Nat. Mater.* **2004**, 3, 545.
- [2] a) S. Zhang, Y. Sunami, H. Hashimoto, *Nanomaterials* **2017**, 7, 246; b) R. R. Costa, J. F. Mano, *Chem. Soc. Rev.* **2014**, 43, 3453; c) T. Fujie, *Polym. J.* **2016**, 48, 773.
- [3] Y. Haraguchi, T. Shimizu, T. Sasagawa, H. Sekine, K. Sakaguchi, T. Kikuchi, W. Sekine, S. Sekiya, M. Yamato, M. Umezu, T. Okano, *Nat. Protoc.* **2012**, 7, 850.
- [4] a) S. J. Benight, C. Wang, J. B. H. Tok, Z. A. Bao, *Prog. Polym. Sci.* **2013**, 38, 1961; b) L. Ricotti, T. Fujie, *Bioinspiration Biomimetics* **2017**, 12, 021001.
- [5] a) D. H. Kim, N. S. Lu, R. Ma, Y. S. Kim, R. H. Kim, S. D. Wang, J. Wu, S. M. Won, H. Tao, A. Islam, K. J. Yu, T. I. Kim, R. Chowdhury, M. Ying, L. Z. Xu, M. Li, H. J. Chung, H. Keum, M. McCormick, P. Liu, Y. W. Zhang, F. G. Omenetto, Y. G. Huang, T. Coleman, J. A. Rogers, *Science* **2011**, 333, 838; b) J. Sugano, T. Fujie, H. Iwata, E. Iwase, *Jpn. J. Appl. Phys.* **2018**, 57, 06HJ04.
- [6] A. W. Feinberg, A. Feigel, S. S. Shevkoplyas, S. Sheehy, G. M. Whitesides, K. K. Parker, *Science* **2007**, 317, 1366.
- [7] a) D. Falconnet, G. Csucs, H. M. Grandin, M. Textor, *Biomaterials* **2006**, 27, 3044; b) A. P. Quist, S. Oscarsson, *Expert Opin. Drug Discovery* **2010**, 5, 569.
- [8] a) R. Ogaki, M. Alexander, P. Kingshott, *Mater. Today* **2010**, 13, 22; b) E. A. Cavalcanti-Adam, T. Volberg, A. Micoulet, H. Kessler, B. Geiger, J. P. Spatz, *Biophys. J.* **2007**, 92, 2964; c) J. Huang, S. V. Gräter, F. Corbellini, S. Rinck, E. Bock, R. Kemkemer, H. Kessler, J. Ding, J. P. Spatz, *Nano Lett.* **2009**, 9, 1111; d) A. I. Teixeira, G. A. Abrams, P. J. Bertics, C. J. Murphy, P. F. Nealey, *J. Cell Sci.* **2003**, 116, 1881; e) M. Mrksich, *Chem. Soc. Rev.* **2000**, 29, 267.
- [9] a) W. Srituravanich, N. Fang, C. Sun, Q. Luo, X. Zhang, *Nano Lett.* **2004**, 4, 1085; b) M. Manso, P. Rossini, I. Malerba, A. Valsesia, L. Gribaldo, G. Ceccone, F. Rossi, *J. Biomater. Sci., Polym. Ed.* **2004**, 15, 161.
- [10] a) E. Delamarche, A. Bernard, H. Schmid, A. Bietsch, B. Michel, H. Biebuyck, *J. Am. Chem. Soc.* **1998**, 120, 500; b) S. Javaherian, K. A. O'Donnell, A. P. McGuigan, *PLoS One* **2011**, 6, e20909.
- [11] a) I. S. Carrico, S. A. Maskarinec, S. C. Heilshorn, M. L. Mock, J. C. Liu, P. J. Nowatzki, C. Franck, G. Ravichandran, D. A. Tirrell, *J. Am. Chem. Soc.* **2007**, 129, 4874; b) M. Shelly, S.-I. Lee, G. Suarato, Y. Meng, S. Pautot, *Methods Mol. Biol.* **2017**, 1493, 321.
- [12] Y. Xia, G. M. Whitesides, *Angew. Chem.* **1999**, 37, 551.
- [13] E. Roth, T. Xu, M. Das, C. Gregory, J. Hickman, T. Boland, *Biomaterials* **2004**, 25, 3707.
- [14] a) J. L. Charest, M. T. Eliason, A. J. García, W. P. King, *Biomaterials* **2006**, 27, 2487; b) A. Bernard, J. P. Renault, B. Michel, H. R. Bosshard, E. Delamarche, *Adv. Mater.* **2000**, 12, 1067.
- [15] a) L. T. de Jonge, S. C. G. Leeuwenburgh, J. J. J. P. van den Beucken, J. G. C. Wolke, J. A. Jansen, *Adv. Funct. Mater.* **2009**, 19, 755; b) C. Muderrisoglu, M. Saveleva, A. Abalymov, L. Van der Meer, A. Ivanova, V. Atkin, B. Parakhonskiy, A. G. Skirtach, *Adv. Mater. Interfaces* **2018**, 5, 1800452.
- [16] a) Y. Haraguchi, T. Shimizu, M. Yamato, T. Okano, *RSC Adv.* **2012**, 2, 2184; b) Q. Ke, X. Wang, Q. Gao, Z. Wu, P. Wan, W. Zhan, J. Ge, Z. Wang, *J. Tissue Eng. Regen. Med.* **2011**, 5, 138; c) M. Kawecki, M. Kraut, A. Klama-Baryła, W. Łabuś, D. Kitala, M. Nowak, J. Gliki, A. L. Sieroń, A. Utrata-Wesołek, B. Trzebicka, A. Dworak, D. Szveda, *J. Mater. Sci.: Mater. Med.* **2016**, 27, 111; d) A. Forghani, L. Kriegh, K. Hogan, C. Chen, G. Brewer, T. B. Tighe, R. Devireddy, D. Hayes, *J. Biomed. Mater. Res., Part A* **2017**, 105, 1346.
- [17] K. Ng, B. Gao, K. W. Yong, Y. Li, M. Shi, X. Zhao, Z. Li, X. Zhang, B. Pingguan-Murphy, H. Yang, F. Xu, *Mater. Today* **2017**, 20, 32.
- [18] a) J. L. Ifkovits, H. G. Sundararaghavan, J. A. Burdick, *J. Visualized Exp.* **2009**, 32, 1589; b) C. Chen, B. T. Mehl, S. A. Sell, R. S. Martin, *Analyst* **2016**, 141, 5311; c) X. M. Mo, C. Y. Xu, M. Kotaki, S. Ramakrishna, *Biomaterials* **2004**, 25, 1883; d) X. Wang, B. Ding, B. Li, *Mater. Today* **2013**, 16, 229.
- [19] a) H. Cao, T. Liu, S. Y. Chew, *Adv. Drug Delivery Rev.* **2009**, 61, 1055; b) Q. Cheng, B. L. P. Lee, K. Komvopoulos, S. Li, *Biomacromolecules* **2013**, 14, 1349.
- [20] a) A. Folch, B. H. Jo, O. Hurtado, D. J. Beebe, M. Toner, *J. Biomed. Mater. Res.* **2000**, 52, 346; b) S. Halldorsson, E. Lucumi, R. Gómez-Sjöberg, R. M. Fleming, *Biosens. Bioelectron.* **2015**, 63, 218; c) K. Kolind, K. W. Leong, F. Besenbacher, M. Foss, *Biomaterials* **2012**, 33, 6626.
- [21] T. Fujie, S. Ahadian, H. Liu, H. X. Chang, S. Ostrovidov, H. K. Wu, H. Bae, K. Nakajima, H. Kaji, A. Khademhosseini, *Nano Lett.* **2013**, 13, 3185.
- [22] T. Fujie, A. Desii, L. Ventrelli, B. Mazzolai, V. Mattoli, *Biomed. Microdevices* **2012**, 14, 1069.
- [23] Y. Okamura, K. Kabata, M. Kinoshita, D. Saitoh, S. Takeoka, *Adv. Mater.* **2009**, 21, 4388.
- [24] S. G. Caridade, C. Monge, F. Gilde, T. Boudou, J. F. Mano, C. Picart, *Biomacromolecules* **2013**, 14, 1653.
- [25] P. Hassanzadeh, M. Kharaziha, M. Nikkhal, S. R. Shin, J. Jin, S. He, W. Sun, C. Zhong, M. R. Dokmeci, A. Khademhosseini, M. Rolandi, *J. Mater. Chem. B* **2013**, 1, 4217.
- [26] A. Perl, D. N. Reinhoudt, J. Huskens, *Adv. Mater.* **2009**, 21, 2257.
- [27] a) J. G. Hardy, L. M. Römer, T. R. Scheibel, *Polymer* **2008**, 49, 4309; b) B. Kundu, N. E. Kurland, S. Bano, C. Patra, F. B. Engel, V. K. Yadavalli, S. C. Kundu, *Prog. Polym. Sci.* **2014**, 39, 251.
- [28] G. H. Altman, F. Diaz, C. Jakuba, T. Calabro, R. L. Horan, J. Chen, H. Lu, J. Richmond, D. L. Kaplan, *Biomaterials* **2003**, 24, 401.
- [29] H. J. Jin, S. V. Fridrikh, G. C. Rutledge, D. L. Kaplan, *Biomacromolecules* **2002**, 3, 1233.
- [30] a) E. S. Gil, S. H. Park, J. Marchant, F. Omenetto, D. L. Kaplan, *Macromol. Biosci.* **2010**, 10, 664; b) M. Hronik-Tupaj, W. K. Raja, M. Tang-Schomer, F. G. Omenetto, D. L. Kaplan, *J. Biomed. Mater. Res., Part A* **2013**, 101, 2559.

- [31] a) N. E. Kurland, T. Dey, S. C. Kundu, V. K. Yadavalli, *Adv. Mater.* **2013**, 25, 6207; b) A. Bucciarelli, R. K. Pal, D. Maniglio, A. Quaranta, V. Mulloni, A. Motta, V. K. Yadavalli, *Macromol. Mater. Eng.* **2017**, 302, 1700110.
- [32] W. Ian, F. Arash, G. B. Alexander, J. Esmaili, K. Ali, *Nanotechnology* **2011**, 22, 212001.
- [33] H. J. Jin, J. Park, V. Karageorgiou, U. J. Kim, R. Valluzzi, D. L. Kaplan, *Adv. Funct. Mater.* **2005**, 15, 1241.
- [34] R. K. Pal, A. A. Farghaly, C. Wang, M. M. Collinson, S. C. Kundu, V. K. Yadavalli, *Biosens. Bioelectron.* **2016**, 81, 294.
- [35] D. N. Rockwood, R. C. Preda, T. Yucel, X. Q. Wang, M. L. Lovett, D. L. Kaplan, *Nat. Protoc.* **2011**, 6, 1612.

**ADVANCED
MATERIALS**
INTERFACES

Supporting Information

for *Adv. Mater. Interfaces*, DOI: 10.1002/admi.201801822

Easy, Scalable, Robust, Micropatterned Silk Fibroin Cell
Substrates

*Meng Xu, Sayantan Pradhan, Francesca Agostinacchio,
Ramendra K. Pal, Gabriele Greco, Barbara Mazzolai, Nicola
M. Pugno, Antonella Motta, and Vamsi K. Yadavalli**

Supporting Information

Easy, Scalable, Robust, Micropatterned Silk Fibroin Cell Substrates

Meng Xu,^a Sayantan Pradhan,^a Francesca Agostinacchio,^b Ramendra K Pal,^a Gabriele Greco,^{c,d}

Barbara Mazzolai,^d Nicola M. Pugno,^{c,e,f} Antonella Motta,^b Vamsi K Yadavalli^{*,a}

| Cycle number | Young Modulus (GPa) | Max Strain (mm/mm) |
|--------------|---------------------|--------------------|
| 1° | 0.75 | 0.01 |
| 2° | 0.79 | 0.01 |
| 3° | 0.79 | 0.01 |
| 4° | 0.80 | 0.01 |
| 5° | 0.79 | 0.01 |

Table S1: Young Modulus at each loading cycle at an imposed maximum strain of 1%.

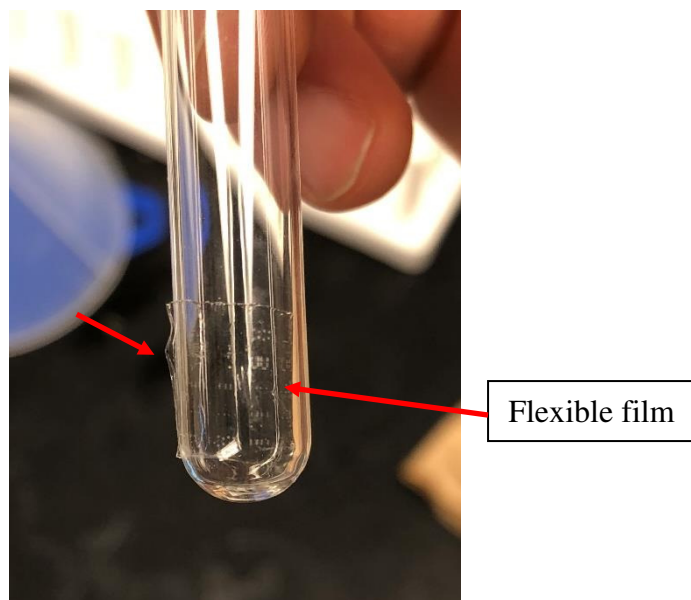
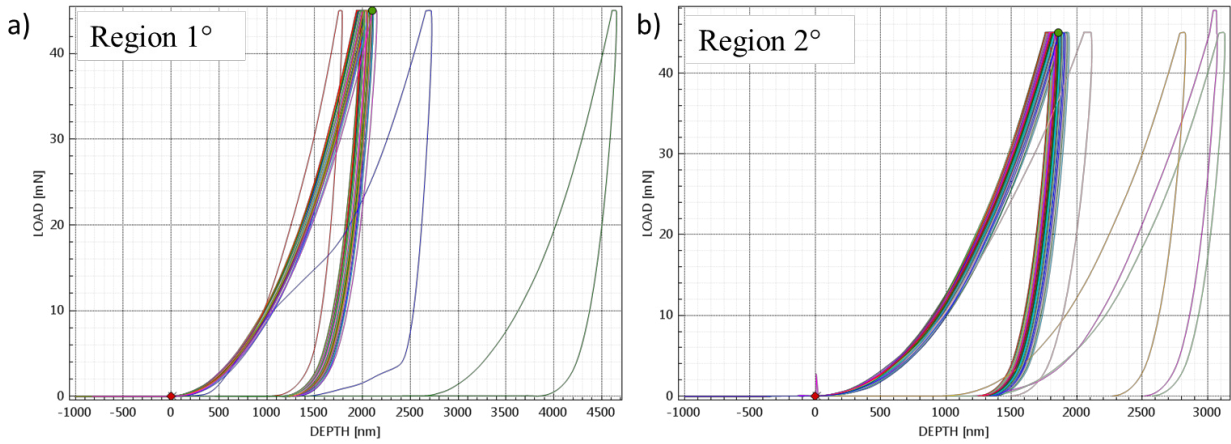


Figure S1 – Flexible micropatterned films can be attached to a curved surface even in dry condition.



c)

| Region | Number of indentation | Young modulus (GPa) | T- Student at 95% | Hardness (GPa) |
|--------|-----------------------|---------------------|----------------------------|----------------|
| 1° | 42 | 8.5±1.5 | 8.03μ8.97 | 0.35±0.07 |
| 2° | 49 | 11.2±3.0 | 10.33μ12.06 | 0.39±0.10 |

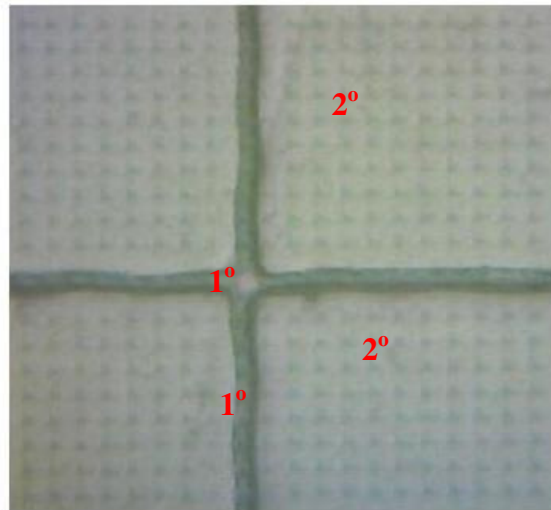


Figure S2: a) Load-displacement curves for indentation in a selected zone of the substrate corresponding to the pattern (Region 1°); b) Load-displacement curves for a different zone of the substrate (Region 2°). c) Values of the obtained Young Modulus and Hardness of the two regions. The T-Student interval of confidence at 95% emphasizes the difference in the mechanical properties of the two regions. The lower panel shows the two regions.

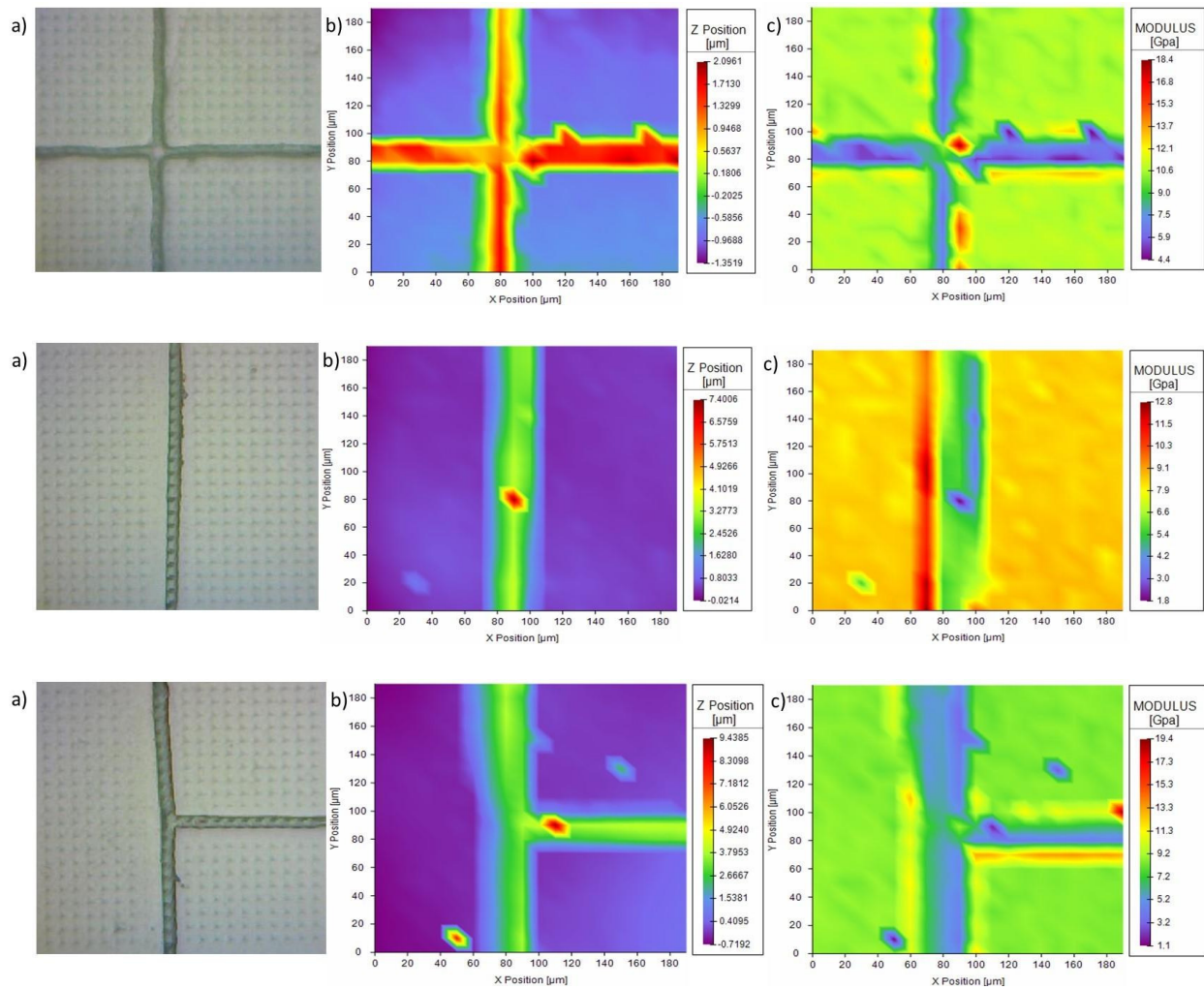


Figure S3: a) The optical microscope picture of 3 patterned regions after the nanoindentations; b) the vertical profile of the patterned substrate and c) its Young Modulus distribution.

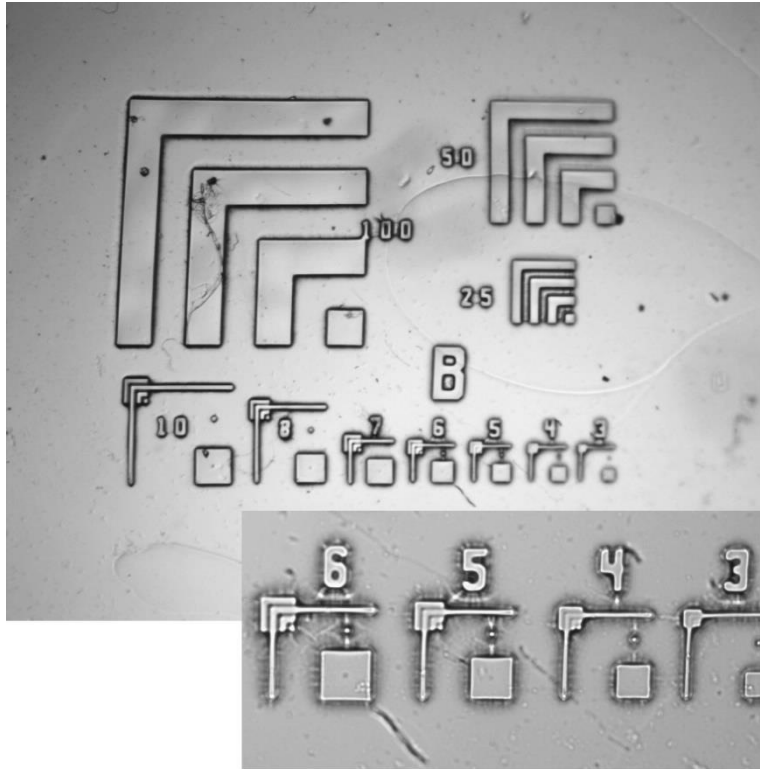


Figure S4 – Optical image of micropatterned films showing the high resolution of patterns formed by photolithography. The numbers on the test pattern refer to the scale in micron. Feature sizes down to a few microns can be easily formed on flexible fibroin protein films. Some parts appear to be out of focus due to the bending of the film.

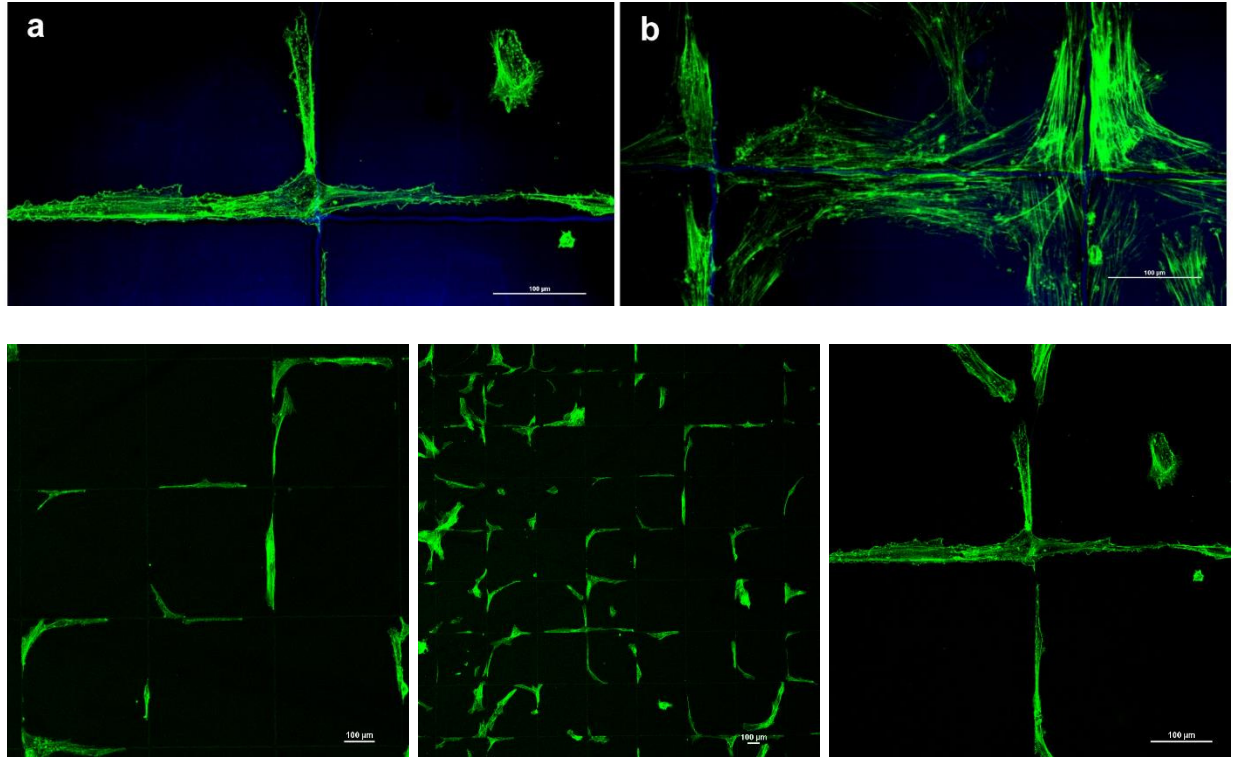


Figure S5: Top: (a) pre-conditioned with complete expansion medium, As a comparison - (b) fibronectin coated films. Scale bar – 100 μm .

Bottom: Additional images of hBM-MSCs adhesion on films preconditioned with complete expansion medium.

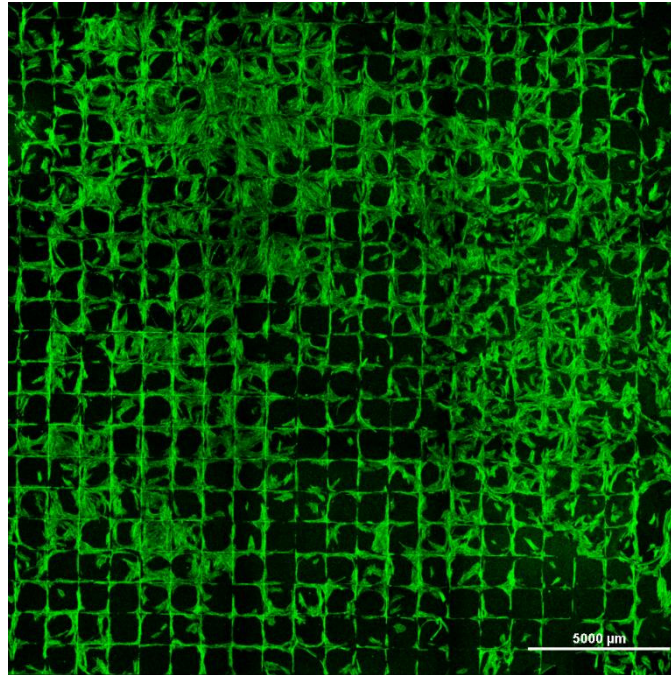


Figure S6: Large area imaging showing attachment of the cells along the microscale grid patterns.